Study of a Low Voltage DC Micro Grid Based on a Solid-State Transformer Under Different Operating Conditions in Smart Grid Distribution

Marwa Chalbi*‡ (iD), Randa Kallel** (iD), Ghada Boukettaya* (iD)

* Department of Electrical Engineering, University of Sfax National School of Engineering, Bpw, 3038, Sfax, Tunisia

** Private Polytechnic Institute of Advanced Sciences of Sfax, 3002 Sfax, Tunisia

(Marwa.chalbi@hotmail.fr, randa.kallel@ipsas.tn, ghada.boukettaya@enis.tn)

‡
Corresponding Author; Marwa Chalbi, 3064 Sfax, Tel: +216 26953410, marwa.chalbi@hotmail.fr

Abstract- This study focuses on developing a suitable control strategy to control a Low Voltage DC (LVDC) distribution system based on a three-stage Solid State Transformer (SST). The architecture of the proposed system is divided into two main subsystems, namely, the SST and the LVDC microgrid (µG). For the SST topology, the three-stage configuration is recognized as the most reliable and effective, especially when integrated with a smart grid system. It contains three distinct stages, the Modular Multilevel Converter (MMC) at the input, interfaces with a High-Voltage Direct Current (HVDC) grid. The Dual Active Bridge (DAB) converter stands at the middle, providing vital isolation while facilitating voltage transformation. Finally, the three-phase inverter coupled to a low voltage (LV) grid via an RL filter. These three stages of the SST harmonize the exchange of power between different voltage levels and grid systems, enabling a resilient and adaptable energy infrastructure for the distribution systems. The LVDC µG, constituted of 3 subsystems, is connected through the LV output of the SST which increases the efficiency of the overall system, improves power quality by regulating and stabilizing the LVDC µG voltage, and enables the integration of different renewable energies. A global supervisory strategy for the LVDC µG based on SST is also being developed based on a cooperative approach to coordinate the power flow between different components of a smart grid. This control strategy was proposed to ensure optimal operation and performance of the overall system and to enhance the quality of the low DC voltage on the SST side during oscillations in the µG output. The developed control strategy leads to maximize the contribution of the PV energy to satisfy the load demand and, therefore, minimizing the reliance of the storage system to extend its lifetime and alleviate the pressure on the main grid.

Keywords Smart grid; Solid state transformer; Dual active bridge converter; Modular multilevel converter; Energy management system.

1. Introduction

Nowadays, electricity has become increasingly important for humankind. Indeed, access to electricity guarantees better living conditions (health, education, etc.) and is a key factor in economic development. The strong industrialization of recent decades and the proliferation of electrical household devices (heating, air conditioning, medical, and IT) have led to a huge worldwide need for electrical energy. Facing this excessive demand for electricity[1, 2], the need for high integration of distributed energy sources and distributed energy storage devices is a potent solution today to improve efficiency and modernize the utility network [3]. This development of intelligent power grids is widely disseminated as a smart grid, and the term "future smart grid" is drawing special attention.

Despite that, the increasing penetration of renewable systems can stress the current grid by causing voltage variations than the system can resist [4]. Due to this, it is become harder to predict and manage the supply and demand of electricity, including renewable energy production, which can result in an imbalance of energy.

To deal with such a challenge, the smart grid requires greater flexibility. The literature has classified flexibility into three main categories: (i) generation flexibility, (ii) distribution flexibility, and (iii) demand flexibility [5, 6]. These categories have been extensively explored in various studies that focus on integrating renewable energy into smart grids [7-10].

Nomenclature		(i_{gd}, i_{gq})	The direct and quadrature components of the measured current at the phase reactor.

Symbol	Definition	Symbol	Definition
LVDC	Low Voltage DC	(V_{vd_ref}, V_{vq_ref})	The direct and quadrature components of the internal AC reference voltage of the MMC.
DG	Distributed generation	(V_{gd}, V_{gq})	The direct and quadrature components of the AC grid voltage.
SST	Solid State Transformer		
EMS	Energy Management System	(i_{gd_ref}, i_{gq_ref})	The direct and quadrature components of the reference currents measured at the level of inductors.
PV	Photovoltaic		
MMC	Modular Multilevel Converter	V_{diffi_ref}	The reference voltage of the internal imbalance of the phase i of the MMC.
DAB	Dual Active Bridge		
V_{cuitot}/V_{clitot}	Sum of capacitor voltages within an arm	i_{diffi_ref}	The reference current of the internal difference of the phase i of the MMC that circulate between MMC arms
$i_{ui/li}$	Current flowing respectively in the upper and lower arm of the leg i	K_{pidiff}	The proportional gain of (PI_{idiff}) corrector
V_{gi}	AC voltage delivered by the AC grid	K_{iidiff}	The integral gain of (PI_{idiff}) corrector
i_{gi}	Phase currents	W_i^{ε}	The stored energy per leg of a phase i
V_{dc}	The MMC DC voltage input	W_i^{Δ}	The energy difference of a phase i
i_{dc}	The DC currents	p_{DCi}	The power exchanged with the dc bus per phase i
		p_{ACi}	The active power per phase i
i_{diffi}	MMC inner difference current of phase i which circulate between the MMC legs.	$i_{diffACi}$	The AC current component of the internal difference of phase i of the MMC.
V_{diffi}	MMC inner unbalance voltage of phase i which relates to i_{diffi} through MMC leg	$i_{diffDCi-ref}$	The DC component of the reference current of the internal difference of phase i of the MMC
V_{vi}	MMC inner AC voltage of phase i	$PI_{W^{\varepsilon}}$	The proportional gain of the $PI_{W^{\varepsilon}}$ corrector
L_{DAB}	Leakage inductance of the transformer	$K_{iw^{\varepsilon}}$	The integral gain of the $PI_{W^{\varepsilon}}$ corrector
V_{DAB1}, V_{DAB2}	Input and output voltage levels of the DAB converter.	$i_{diffACi-ref}$	The AC component of the reference current of the internal difference of phase i of the MMC
n_{Tr}	Transformer turn ratio	$PI_{W^{\Delta}}$	The proportional gain of the $PI_{W^{\Delta}}$ corrector
d	The DAB phase shift ratio with $d = \frac{\theta}{\pi}$,	$K_{iw^{\Delta}}$	The integral gain of the $PI_{W^{\Delta}}$ corrector
		$V_{DC_{ref}}$	The reference DC voltage

θ	The phase shift in radian between the primary and secondary bridges	K_{pv}	The proportional gain of (PI_v) corrector
f	The switching frequency.	K_{iv}	The integral gain of (PI_v) corrector
V_{md}, V_{mq}	The components of the modulated voltages, including both the direct and quadrature ones.	K_{pdc}	The proportional gain of PI_{Bus} corrector
$V_{dw_{ref}}, V_{qw_{ref}}$	The voltage converter regulations include both the direct and quadrature components.	K_{idc}	The integral gain of PI_{Bus} corrector
i_{td} and i_{tq}	The currents measured at the phase reactor include both the direct and quadrature components.	PV_1, PV_2, PV_3	The power produced by each PV panel 1, 2 and 3.
i_{minv}	The current flow through the converter	P_{bat}	The power supplied to or taken from the battery.
(V_{vd}, V_{vq})	The direct and quadrature components of the internal AC voltage of the MMC.		

In order to ensure the balance between supply and demand and improve the stability of the electricity network, an Energy Management System (EMS) was established [11]. In the smart grid, the EMS is required for the interconnection of power generation, energy storage, and loads, and it must ensure bidirectional energy flows. In this context, a large amount of research has been conducted to develop the EMS to improve reliability, increase productivity and stability of the grid, mitigate the power generation cost, and maximize the utilization of renewable energy sources to ensure optimal system efficiency [5, 11, 12]. These different changes in the grid have motivated the development and implementation of Power Electronic Devices (PEDs) in distribution systems rather than conventional transformers (CTs) [13-15]. Hence, the use of a new concept of transformer named SST to satisfy the needs of the current network is unavoidable [12]. This concept, introduced in 1970, was primarily involved solid-state switches with high-frequency isolation and solved all the issues of the CTs [16]. Although the concept of SST has been revolutionary, its implementation in various applications is very challenging [17, 18]. After many years, the use of suitable semiconductor devices with the new topology configurations begins to become active. This appearance was proposed in the "FREEDM's" center in 2008 [19], and it has gained interest from different companies, including[12, 20], the Electric Power Research Institute (EPRI), Asea Brown Bovari (ABB)[21], and power electronic traction transformer (PETT) [22]. The typical distribution system is shown in Fig. 1, includes the transformer required for operating traction or locomotive systems and for connecting FACTs components such active power filters and reactive power compensators. For applications involving the smart grid, the SST serves as a high potential replacement for the conventional transformer due to its numerous advantages and capabilities. For example, it offers enhanced flexibility and efficiency in the distribution network, achieved through power electronics and advanced control algorithms, it enables real-time voltage regulation, two-way power control, and the direct integration of renewable energy systems with the distribution grid. Their compact size and weight further facilitate easier integration into various applications, allowing for more efficient power distribution and enhanced system performance. In contrast, CTs are passive devices that are unable to manage the bidirectional power flow and information between the power grid and consumers. They are also easily affected by unbalanced voltage conditions caused by the integration of DERs. Furthermore, CTs encounter problems related to their heavy weight, sensitivity to harmonic distortions, and susceptibility to electrical stress [15, 16].
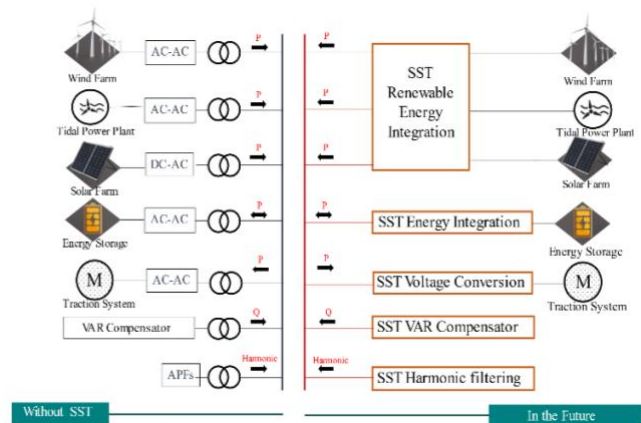
Fig.1. SST applications in distribution system.

Choosing the most appropriate topology for the SST is a highly complex and demanding task. In this context, several available topologies for SST have been studied and classified into three categories according to the number of power conversion stages: (i) single-stage, (ii) two-stage, and (iii) three-stage [16, 23]. The most practical and viable choice among the available topologies is the three-stage design featuring two DC links. This option stands out due to its high flexibility, high control performance, and its ability to effectively utilize modular multilevel converters on the High voltage (HV) side. Moreover, it allows for seamless integration with a DC distribution system, making it possible to supply power to DC loads and interconnect Distributed Generation (DG) systems like PV panels and energy storage units [24]. Additionally, this design adequately fulfills power demand and voltage regulation requirements at the LV grid side, ensuring a stable and reliable power supply [13, 14, 16].

Several studies focus on the application of three stages SST converter for a µG battery and PV systems. Before doing so, a literature review of the more recent works dealing with the smart grid system based on SST application is presented hereunder.

Reference [25] presents a control strategy designed for a Phase-Separated Configuration Three-Phase Solid-State Transformer aimed to minimize the necessity for energy storage capacitors. Reference [26] improves the topology of SST to be integrated into smart distribution networks and proposed a practical hierarchical control strategy enhances the issue of voltage stability caused by the fluctuations of renewable energy generation. Authors in reference [27] propose a decentralized grid edge voltage control method without the need for a grid model, coupled with a day-ahead Battery Energy Storage System (BESS) dispatch method, specifically designed for the SST and hybrid transformer. Reference [28] puts forward a current source DC-SST solution designed for MVDC hybrid systems containing wind turbines, PV panels, and energy storage farms. A scheme is presented to decrease the number of devices on the DC link current path by adopting a specific technique on reverse-blocking device bridges. Reference [29] presents a bidirectional DCSST operating with three-level power modules to interconnect DC medium voltages (MVDC) and low voltages (LVDC).

The present paper aims to develop a suitable control strategy using an energy cooperative approach to manage power sharing for LVDC systems based on SST. This new architecture integrates the three-stage SST and provides both DC and AC supplies. In the proposed architecture, a µG was connected at the DC side of the SST. To control the DC bus voltage and enhance the PV system's performance, the microgrid (µG) integrates an energy storage system connected to the DC bus through a DC/DC converter. In order to maintain the necessary power flow, PV arrays are further connected to the DC bus via its own DC/DC converter. Finally, unbalanced AC loads are coupled to the DC bus using a separate DC/AC converter. The presence of SST in this architecture improves power quality management, enhances the grid flexibility and

stability, enables advanced fault detection capability, and allows for the uncoupling of the bus from the other side of the load [30]. These capabilities contribute to the efficient, reliable, and sustainable operation of the smart grid. They enable the seamless integration of renewable energy resources and storage systems, enhance grid resilience, and improve the overall performance of the electrical system. The proposed control method was made in order to enhance the SST's DC voltage quality when dealing with oscillations in the microgrid's output voltage. The control loop in this study also helps to alleviate the current imbalance across the capacitor brought on by the different power behavior speeds of the MMC and the DAB. In addition to the issue of power variation in the microgrid, this adaptable control method is also appropriate for other types of transient circumstances, such as microgrid isolation under fault conditions [5, 26]. For this purpose, a supervision algorithm was created to fulfill the load power constraint. The remaining sections of this paper were organized in the following way: The architecture of the LVDC system based on SST was elaborated in Section 2, the model of the different conversion stages of the three-stage topology and the control strategy were detailed in section 3 and 4, The elaboration on the power management algorithm took place in Section 5, simulation results are then provided in section6 to prove the effectiveness of the proposed strategy. Finally, section7 concludes this article.

2. Description of the LVDC Microgrid Based SST

Microgrid architectures are based on either AC or DC buses, or a combination of both [31]. Generally, the usual voltage in micro-grid is less than the Medium Voltage (MV) in a grid distribution system. Thus, the integration of AC and DC microgrids necessitates the use of an additional transformer to link them to the MV distribution system. [32]. As the CTs does not meet the demand for microgrids, the SST is shown as a promising solution for microgrid architecture. For that reason, in this work, we adopt the "SST-based LVDC microgrid" topology as depicted in Fig. 2. The SST operates as a central energy core, balancing the power flow among the main grid, the DC microgrid, and the residential LVAC load. The DC microgrid consists of photovoltaic power supplies, an energy storage device, and an unbalanced AC load. It is linked to the main grid via the 400 V LVDC port located on the SST side.
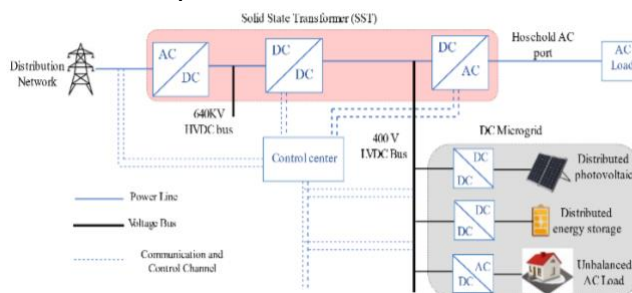
Fig. 2. Topology of a DC microgrid system based on SST.

The architecture of the proposed LVDC distribution system based on SST is depicted in Fig. 3. The proposed configuration encompasses two main components noted,
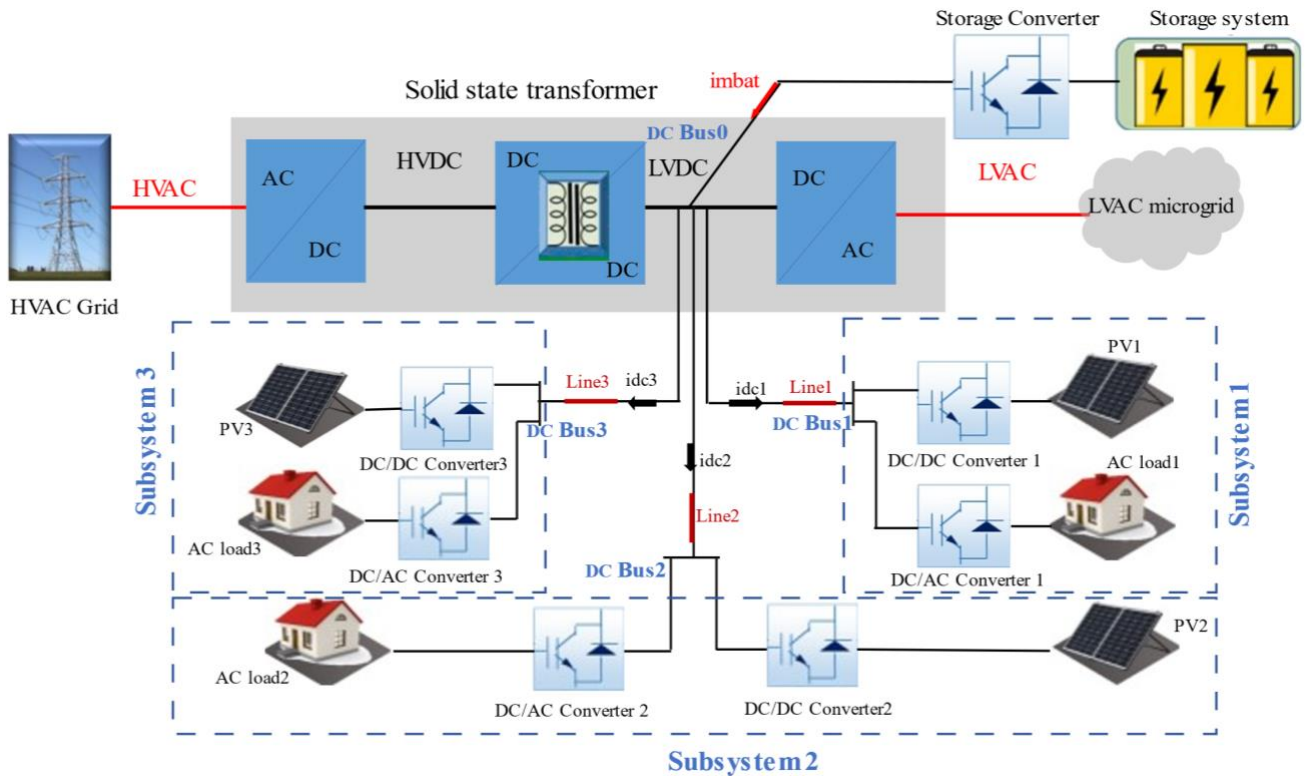
Fig. 3. Configuration of the overall LVDC distributed system.

the SST and the LVDC microgrid. The SST adopts the MMC as its input stage, which is responsible for the voltage stability of the HVDC bus. Additionally, a DAB is integrated as the isolation stage to ensure voltage stability in the LVDC bus. Lastly, a three-phase inverter acts as the output stage to provide the alternating voltage at the desired frequency [26]. In the LVDC μG we adopt a star connection structure. A PV array, a DC/DC converter, and an AC load through a DC/AC converter are all used to simultaneously connect each DC bus to an AC load. A shared energy storage component of the system is linked to DC bus 0 by a DC/DC converter. In fact, to enable power sharing amongst the various subsystems, all of the DC buses are interconnected. The effective implementation of the power management strategy is ensured by controlling the power flow among the different buses. The load and storage system should both be able to receive power from the PV system through this system. Sharing the battery under various operating situations allows this system to transfer extra power or absorb a lack of power, which is one of its most crucial features. An EMS has been created to regulate the power transfer within a cluster consisting of an AC grid and an LVDC microgrid. The main objective is to ensure power balance and a constant voltage at each DC bus under various required power levels [33]. The LVDC side of the SST is linked to the LVDC microgrid system. As a result, the SST fixes the local grid's impedance matching issue [34]. Additionally, it enables the seamless integration of renewable sources and energy storage devices, contributing to the mitigation of volume and complexity challenges faced by conventional systems. The performance of the suggested architecture under various operating conditions and disturbances will be evaluated using computational simulations in the MATLAB/Simulink software.

3. Model of the Different Conversion Stages of Three Stage SST Topology

3.1. Model of the AC/DC Conversion Stage

The HV converter stage converts the HVAC to HVDC through a rectifying process. The primary objective of this converter is to absorb active power from the distributed grid to supply the next stage and manage reactive power for grid services. Adopting a multilevel topology is the most efficient approach to design this converter [33, 35]. There are three available topologies: the Neutral Point Clamped (NPC), the MMC, and the Cascaded H-bridge (CHB). Based on literature and recent studies, the MMC has emerged as a preferred topology for HV conversion due to its uncomplicated structure involving a small number of power devices [36]. The topology consists of three legs, with each leg further divided into two arms. The upper arm (u) and low arm (l) are terms used to describe the arms that are attached to the positive bar and the negative bar, respectively. A series inductor (R_{arm}, L_{arm}) and a collection of submodules are present in each arm to limit the inrush and circulating current during start-up and steady-state operations due to the instantaneous voltage difference between the arms [36, 37].

Depending on the type of application, different numbers of submodules are connected in series. The MMC needs 200–400 SM/arm in the current HVDC transmission system in order to attain +/– 320 KV on the DC side of the arm. We can simplify the modeling and control of an MMC by separating the issue of capacitor voltage balancing inside

each arm [36, 37]. Fig. 4 depicts the MMC utilizing the arm average model.
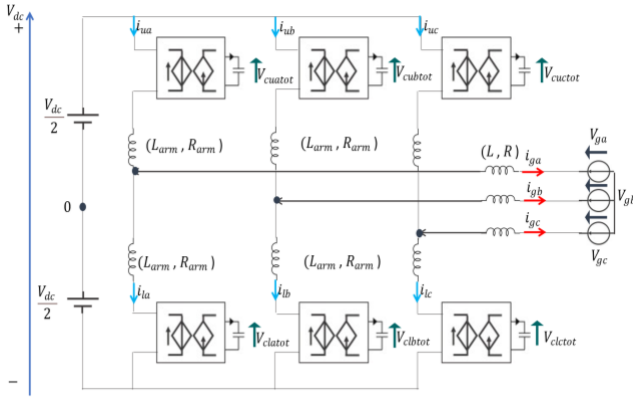
Fig. 4. MMC developed from the arm-average model.

We identified 11 autonomous state variables in the modular multilevel converter including:

- Six voltages ($V_{cua_{tot}}$, $V_{cla_{tot}}$, $V_{cub_{tot}}$, $V_{clb_{tot}}$, $V_{cuc_{tot}}$, $V_{clc_{tot}}$)

- Three arm current (i_{ua}, i_{ub}, i_{uc})

- Two phase current (i_{ga}, i_{gb})

Through the application of Kirchhoff's current and voltage equations to the upper and lower loops of the MMC, it becomes feasible to represent the MMC using a matrix form. The matrix diagonalization process results in the subsequent variable transformations:

$$\begin{cases} i_{diffi} = \dfrac{i_{ui} + i_{li}}{2} \\ V_{diffi} = \dfrac{V_{mui} + V_{mli}}{2} \\ V_{vi} = \dfrac{V_{mli} - V_{mui}}{2} \end{cases} \tag{1}$$

Two decoupled equations describe the system:

$$\frac{V_{dc}}{2} - V_{diffi} = L_{arm} \frac{di_{diffi}}{dt} + R_{arm} i_{diffi} \tag{2}$$

$$V_{vi} - V_{gi} = \left(L + \frac{L_{arm}}{2} \right) \frac{di_{gi}}{dt} + \left(R + \frac{R_{arm}}{2} \right) i_{gi} \tag{3}$$

3.2. Model of the DC/DC Conversion Stage

The DC/DC is considered as an integral part of the SST applications to control the bidirectional power transfer, between the HVDC bus and the LVDC bus, by regulating the DC bus voltages. The core component of this stage is the High Transformer, which plays a crucial role in reducing volume and achieving electrical isolation [38]. The DC/DC stage can be divided into 3 parts: at the input, there is a DC/AC inverter, followed by a high-frequency transformer in the middle, and finally, an AC/DC converter at the output. Moreover, many existing topologies of IBDC receive more attention from researchers and be suitable for SSTs applications, such as Serie Resonant Converter (SRC), Dual

Half-bridge converter (DHB) or DAB [14]. The DAB converter is the most adopted one for SST applications due to its simple structure, high power density, and capability of bi-directional power flow [39]. The implemented configuration of the DAB converter is illustrated in Fig. 5.

It comprises of two H-bridges joined by a high-frequency transformer and powered by DC buses. Each module's high voltage side of the DAB is connected to each MMC arm's submodule by a HVDC link, and all of the module's low voltage sides are paralleled at an LVDC bus [39-41].
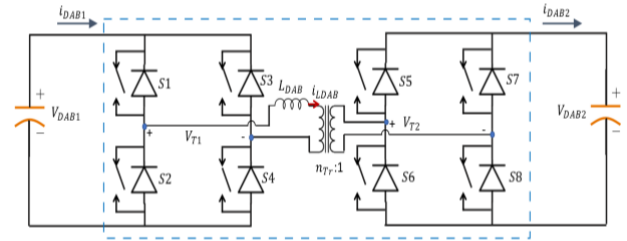
Fig. 5. DAB converter topology.

At the transformer terminals, each H-bridge is controlled to generate a two-level square waveform with a 50% duty cycle. By regulating the phase shift (θ) between the high DC voltage (V_{DAB1}) and low DC voltage (V_{DAB2})waveforms, the converter's output power can be regulated. To improve power transfer management, it may be necessary to include an auxiliary inductance (L_{DAB}) in series with the transformer, depending on the converter power ratings [42]. High-frequency switching will be used to minimize the size of passive components. The isolation transformer's magnetizing inductance is minimal at high frequencies, and the transformer can only be represented by its leakage inductance [43].

Multiple modulation methods can be used to minimize losses and boost efficiency across a wide operating voltage range due to the flexibility provided by the DAB's primary and secondary active bridges. Under the Single Phase Shift (SPS) modulation, the full-bridge converters are controlled with a constant switching frequency and maximum duty cycles limited to 0.5, Moreover, the bridge leading with a phase shift, represented by θ, transfers power to the trailing one [40]. The power flow in the converter at steady state is mathematically described by the following equation: [44-46]

$$P_{DAB} = \frac{V_{DAB1}.V_{DAB2}.d.(1-|d|)}{2.L_{DAB}.f.n_{Tr}} \tag{4}$$

The average terminal currents can be representing as follows:

$$i_{DAB1} = \frac{n_{Tr} V_{DAB2} \, d(1-|d|)}{2L_{DAB}f}, \; i_{DAB2} = \frac{n_{Tr} V_{DAB1} \, d(1-|d|)}{2L_{DAB}f} \tag{5}$$

When the phase shift d is positive, power is transferred from V_{DAB1} to V_{DAB2}. If the power flows in the opposite direction, from V_{DAB2} to V_{DAB1}, the directions of all dependent currents in the model are reversed [44, 45, 47].

3.3. Model of the DC/AC Conversion Stage
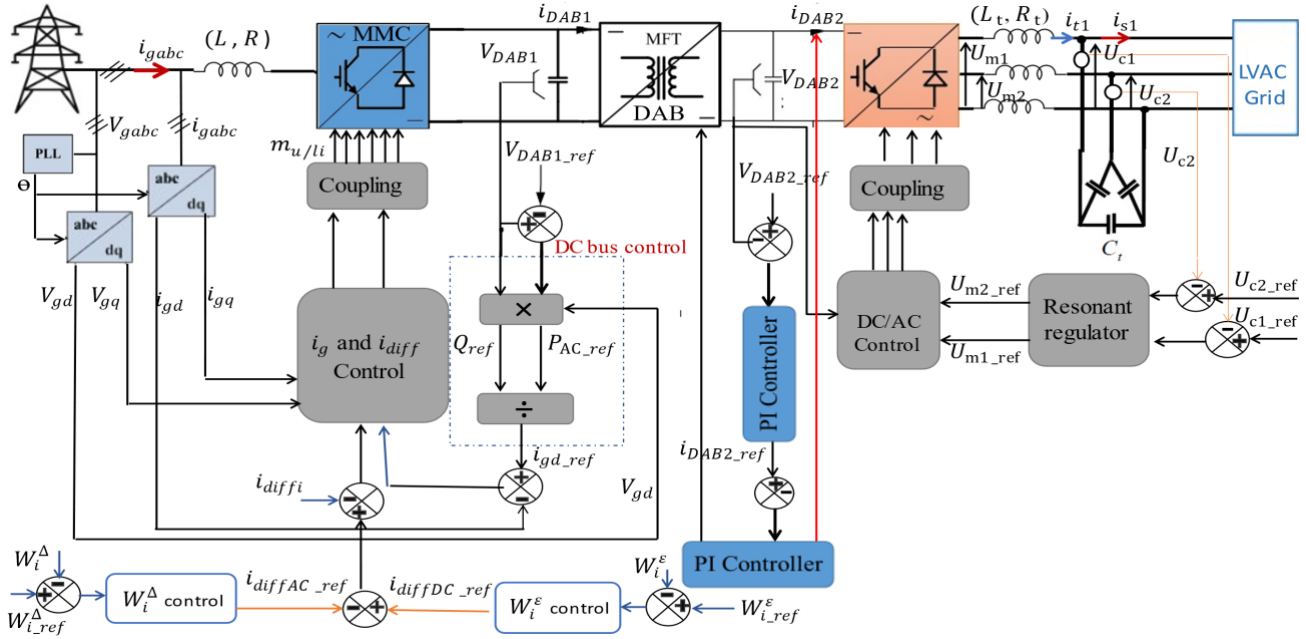
Fig. 6. A general structure of the control strategy.

The three-phase voltage converter consists of three parallel legs. In each leg, there are two switches: a high and a low switch, which are bidirectional in current and unidirectional in voltage. For continuous operation mode, the switching cell consists of an IGBT switch with an anti-parallel freewheel diode. A balanced three-phase system (voltages and currents) in the Park coordinate system has been utilized to create an equivalent continuous model of the converter. In the Park coordinate system, the single voltages modulated by the converter on the grid side depend on the converter control voltages. The corresponding equations for these modulated voltages are as follows:

$$V_{md} = V_{dw_{ref}} \frac{V_{DAB2}}{2}, \quad V_{mq} = V_{qw_{ref}} \frac{V_{DAB2}}{2} \tag{6}$$

The equation representing the modulated current of the studied inverter is presented below:

$$i_{m_{inv}} = \frac{1}{2} \left(V_{dw_{ref}} i_{td} + V_{qw_{ref}} i_{tq} \right) \tag{7}$$

4. Control of the Different Conversion Stages of Three Stage SST Topology

The proposed control strategy is shown in Fig. 6. It depicts the three main stages of the SST: the input stage, isolation stage, and output stage. The input stage employs an MMC due to its benefits, including bidirectional power flow, unity power factor, and control over DC bus voltage. To mitigate high current harmonics, this rectifier is linked to a symmetrical and balanced high voltage grid through a passive filter. The choice of the filter is made for its ability to minimize current harmonics while reducing filter size and cost. The isolation stage is based on the DAB converter, comprising full-bridge circuits on both the primary and secondary sides, interconnected by a medium-frequency transformer. This configuration offers numerous benefits,

including a reduced requirement for passive components, reduced electromagnetic interference, bidirectional power flow, and high flexibility. The output stage consists of a three-phase inverter connected to a low-voltage (LV) grid via the LC filter. This configuration serves to reduce current harmonics, smooth the output waveform, minimize voltage distortions, and ensure the generation of sinusoidal waveforms. The three stages of the SST work together to efficiently convert, transform, and distribute electrical power, making it an advanced and versatile solution for modern distribution systems, renewable energy integration, and grid management.

4.1. Control of the Modular Multilevel Converter
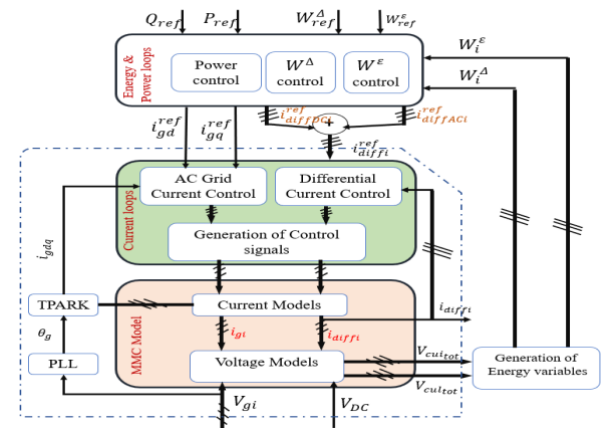
Fig. 7. A general configuration of the MMC control bloc diagram.

In order to achieve control of the MMC-HVDC system, the number of controllers must match the number of independent state variables (11 state variables) in the entire system. The "energy-based control" method has been

designed and presented in Fig. 7. With this approach, all state variables of the system are regulated. The main control design comprises two parts: the inner control loop, which is further divided into AC Current Control and Differential Control, and the outer control loop, which encompasses power, voltage, and energy control.[36]

The description of the system after applying the Park transformation is shown as follow:

$$V_{vd} - V_{gd} = \left(L + \frac{L_{arm}}{2}\right)\frac{di_{gd}}{dt} + \left(R + \frac{R_{arm}}{2}\right)i_{gd} + \left(L + \frac{L_{arm}}{2}\right)wi_{gq} \tag{8}$$

$$V_{vq} - V_{gq} = \left(L + \frac{L_{arm}}{2}\right)\frac{di_{gq}}{dt} + \left(R + \frac{R_{arm}}{2}\right)i_{gd} - \left(L + \frac{L_{arm}}{2}\right)wi_{gd} \tag{9}$$

The implemented regulator (PI) is designed as Pig,

with $PI_{igd} = PI_{igq} = PI_{igi}$

$$V_{vd\_ref} = V_{gd} + \left(i_{gd\_ref} - i_{gd}\right) - \left(\frac{L_{arm}}{2} + L\right)wi_{gq} \tag{10}$$
$$\tag{9}$$
$$V_{vq\_ref} = V_{gq} + \left(i_{gq\_ref} - i_{gq}\right) + \left(\frac{L_{arm}}{2} + L\right)wi_{gd} \tag{11}$$

+ The differential current in each phase is regulated by another controller (PI_{idiff}).

From equation (2), the current control i_{diff} for phase i is derived such that:

$$V_{diffi-ref} = \frac{V_{dc}}{2} - \left(i_{diffi-ref} - i_{diffi}\right)PI_{idiff} \tag{12}$$

Based on the operating mode (inverter/rectifier), the total energy stored in the MMC can be controlled from either AC or DC terminals. There are two types of energy distribution balancing systems:

- Horizontal balancing, involves the exchange of energy among the legs through appropriate circulating current components, implies the energy's replacement in the horizontal direction.
- Vertical balancing, which is the energy exchange between two branches that belong to the to the same leg, implies the energy replacement in a vertical direction [47].

Equation 11 presents the average values of the stored energy in one period (T) of an MMC leg. It highlights the relationship between the stored energy in the upper arms, lower arms, and the inner currents of the MMC [36].

$$\begin{cases} \langle\frac{dW_i^\varepsilon}{dt}\rangle_T = p_{DCi} - \langle p_{ACi}\rangle_T \\ \langle\frac{dW_i^\Delta}{dt}\rangle_T = -2\langle i_{diffACi}V_{gi}\rangle_T \end{cases} \tag{13}$$

+ The stored energy for each leg (W_{iref}^ε) for phase i is regulated by a proportional integral corrector (PI_{W^ε}) using the following equation:

$$i_{diffDCi-ref} = \frac{1}{V_{DC}}\left[\langle W_{iref}^\varepsilon - W_i^\varepsilon\rangle_T PI_{W^\varepsilon} + \frac{P_{AC}}{3}\right] \tag{14}$$

+ The energy difference (W_{iref}^Δ) for phase i is regulated by a proportional integral corrector (PI_{W^Δ}) in each leg of a phase i using the following equation:

$$i_{diffACi-ref} = \frac{1}{2V_{gi}}\langle W_{iref}^\Delta - W_i^\Delta\rangle_T PI_{W^\Delta} \tag{15}$$

+ The DC bus control is regulated by a proportional integral corrector (PI_v) using the following equation:

$$i_{c-ref} = PI_v(V_{DC_{ref}} - V_{DC}) \tag{16}$$

4.2. Control of the Dual Active Bridge Converter

The DAB converter serves as a connection between the MMC and the three-phase voltage inverter. It plays a crucial role in isolating the HV an LV sides and is responsible for maintaining the input or output voltages at their designated values. The specific voltage controlled by the DAB varies depending on its operating mode. In the buck mode, the DAB ensures a constant value for V_{DAB2}, while in the boost mode, it maintains V_{DAB1}.

Figure 6 depicts the control configuration of the DAB converter when operating in the buck mode, facilitating power transfer from the HV input to the LV output. The DAB's feedback control system comprises an outer voltage loop and an inner current loop. For the current loop's design, it is assumed that the voltage on both sides of the DAB remains constant, allowing the control system to focus on regulating the current flow through the DAB. This design approach ensures stable and efficient operation of the DAB converter and facilitates smooth power transfer between the MMC and the three-phase voltage inverter [34, 45].

4.3. Control of the Three-phase Inverter Connected to the grid

4.3.1. Control of the three-phase inverter
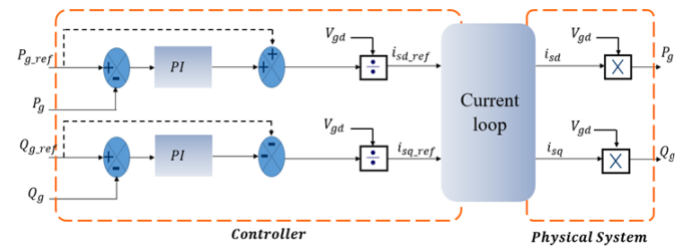
Fig.8. Active and reactive power control loops.

The control of the inverter is done in order to control the transited currents by the filter and keep the DC bus voltage constant. After measuring the DC bus voltage, the converter is controlled to set the output voltages to reference values. Fig. 8 presents the global control of the inverter, including power control and current control. The power controller guarantees the transfer of active and reactive powers at the PCC, especially when the AC filter is not a simple RL circuit. Also, it is used to fix active and reactive power

dynamics responses [48]. With this characteristic, power controllers guarantee that the active and reactive power exchange at the PCC and the power reference dynamics are close to those of the current loop.

4.3.2. Control of LVDC microgrid

As mentioned previously, the system under investigation is a Loop DC Microgrid powered by PV renewable sources, intended to provide electricity to AC loads. The LVDC system consists of three DC buses, each comprising a PV array, a DC/DC converter, an AC load, and a DC/AC inverter. Additionally, a battery bank is linked to one of the buses via a storage converter, and this particular bus has been identified as the optimal location for the battery bank in terms of minimizing losses and maximizing system efficiency. The DC bus0 makes the connection between the battery and the other DC buses respectively (bus1, bus2, and bus3), as shown in Fig.3.

The DC current (i_{dc0}) is influenced by the direction of the modulated current of the Battery storage system, as indicated by the following equation:

$$i_{dc0} = (i_{mbat} + i_{DAB2}) - (i_{dc1} + i_{dc2} + i_{dc3} + i_{minv}) \quad (17)$$

For the LVDC distribution system, The DC bus voltage is controlled by a PI_{Bus} corrector, which regulates the current through the capacitor using the following equation:

$$i_{mbat\_ref} = PI_{Bus}(V_{DAB2}^* - V_{DAB2}) \quad (18)$$

The DC bus receives power from both the battery and the three individual DC buses (bus 1, 2, 3). Therefore, a balance between the different powers exchanged is made at the DC bus to adjust the corresponding voltage. The main objective of the control of the storage system is to fix the i_{bat} current to its reference value. Then, a current regulation loop is performed to regulate the current of the storage system using a PI regulator as presented in Fig. 9.

Fig. 9. Control structure of the DC Bus.

5. Power Flow Management Strategy

The system's configuration relies on the interconnection of various elements through a DC microgrid, allowing them to function in a coordinated manner. This interconnection enables proper power sharing among the components and ensures the stability of the bus voltages. For that reason, the associated power control strategy encourages the notion of energy cooperation among various DGs: this is the adopted control strategy in this paper [32]. As depicted in Fig. 3,

each subsystem is capable of simultaneous communication, enabling interactions not only with the storage system but also with the other subsystems and the LVAC microgrid. In this study, a suitable control strategy was established to effectively manage the power-sharing among a cluster comprising an AC grid supported by a DC supply microgrid. This control technique uses a cooperative approach to supervise the distribution of the energy flows and allow power distribution to different sources. This strategy is based on sharing the PV power among subsystems in a local system connected to the LVAC microgrid to gain from the maximum amount of renewable energy and minimize the use of the storage system. Therefore, an intelligent algorithm was developed to fulfill the load powers, maximize the uses of the PV energy, and check the storage system level under different conditions [38-39]. For that reason, the power flow strategy implementation must consider the following constraints:
- The variation of the PV profiles.
- The variation of the power load demand.
- Preventing battery deep discharge and battery overcharging:
  $$SOC_{min} < SOC < SOC_{max}$$

Where: SOC_{min} and SOC_{max} are respectively, the minimum and maximum SOC limits.

Given the various limitations mentioned above, the algorithm must fulfill the following criteria:
- Enable cooperative coordination among the various subsystems of the LVDC distributed system to facilitate power flow sharing between PV panels and different AC loads, maximizing the utilization of solar energy and enhancing flexibility in load management strategies for the proposed microgrid (μG).
- Maintain a consistent and reliable power delivery to the connected loads.
- Optimize the utilization of the battery storage system to minimize its usage, thereby prolonging battery life and enhancing overall system efficiency.

The power management strategy is developed to achieve both system autonomy and satisfy the defined energy limitations. This algorithm necessitates information about the power generation from the PV panel, the power consumption of the load, and the state of charge of the battery [44]. The total power (PV_t) generated in the studied system, can be expressed as follows:

$$PV_t = PV_1 + PV_2 + PV_3 \quad (19)$$

The total power consumed by the AC unbalanced loads (PL_t), can be represented by the following equation:

$$PL_t = PL_1 + PL_2 + PL_3 \quad (20)$$

PL_1, PL_2, PL_3 : The power requirements of loads 1, 2, and 3, respectively.

To ensure a power balance between different DGs, the power balance equation is governed by the following expression: $PVt + Pgrid + pbat = PLt \quad (21)$

764

Operation of subsystem1

$p_{pvi}(t), p_{Li}(t), p_{pvt}(t), p_{Lt}(t), soc(t)$

Energy Cooperative Approach

$p_{pv1}(t) > p_{L1}(t)$ — Yes / No

$p_{pv2}(t) > p_{L2}(t)$ — No / Yes

$p_{pv2}(t) \leq p_{L2}(t)$ — Yes / No

$p_{pv3}(t) > p_{L3}(t)$ — No / Yes

$p_{pv3}(t) > p_{L3}(t)$ — No / Yes

$p_{pv3}(t) > p_{L3}(t)$ — No / Yes

$p_{pv3}(t) > p_{L3}(t)$ — Yes / No

Transfer Energy to Subsystem 2 and 3 — Case1

Transfer Energy to Subsystem 2 — Case2

Transfer Energy to Subsystem 3 — Case3

Transfer Energy to Subsystem 1 and 3 — Case4

Transfer Energy to Subsystem 1 — Case5

Transfer Energy to Subsystem 1 and 2 — Case6

or

$p_{pvt}(t) > p_{Lt}(t)$ — Yes / No

or

or

$soc > soc_{max}$

$soc > soc_{min}$

Battery charged
$p_{bat}(t) = p_L(t) - p_{pvt}(t)$ — Mode1

Energy transferred to the grid
$p_g(t) = p_L(t) - p_{pvt}(t)$ — Mode2

Battery discharged
$p_{bat}(t) = p_L(t) - p_{pvt}(t)$ — Mode3

Energy covered by the grid
$p_g(t) = p_L(t) - p_{pvt}(t)$ — Mode4

Fig.10. Control structure of the DC Bus.

The control strategy relies on local information and communication among the various subsystems. It aims to regulate power transfer between different system elements and maintain voltage stability on the DC bus. By implementing this control strategy, the system maximizes the utilization of PV energy to supply loads through a cooperative approach among the PV subsystems. This cooperative approach, illustrated by the six cases, enhances the system's efficiency and improves energy utilization and overall performance. The developed algorithm needs to know the instantaneous demand and generated PV powers of each subsystem and the battery state of charge to supervise the power flow in the LVDC distributed under four operational states as presented in Fig. 10.

When the generated PV power associated with subsystem '1' is higher than the corresponding demand power ($PV_1 > PL_1$), different cases will appear:

✓ If the other subsystems have excess power, each subsystem will satisfy its needs and the extra power must be transmitted to charge the battery while its maximum state SOC has not reached yet ($SOC \leq SOC_{max}$): mode 1. If the battery bank is full charged ($SOC = SOC_{max}$), the extra power will be delivered to the local LVAC grid: mode2

✓ If there is a lack of energy in the other subsystems (the load demand is higher than the PV generated power): the extra power of subsystem 1 will be transferred to these subsystems to satisfy their needs. After the energy transfer between subsystems, two cases can exist:

✓ If the loads in the different subsystems in need are satisfied by the transfer of energy, and if there is still a surplus of PV energy, this excess must be transmitted either to the grid or to the battery depending on the SOC as explained in the previous paragraph.

✓ After the transfer of excess energy from subsystem 1 to the subsystems in need, if this surplus energy is insufficient to meet the needs of these subsystems, then the solution is as follows: the battery bank will be discharged to cover this lack of power while its state of charge has not reached its minimum value ($SOC > SOC_{min}$): mode 3. If the battery bank is fully charged ($SOC = SOC_{min}$), the lack of power is covered by the local LVAC grid: mode 4.

6. Simulation Results

In this work, the proposed system has been implemented and simulated in a MATLAB-Simulink environment using the parameters provided in table1. The simulation results were categorized into two primary sections: in the first section, a simulation of the three-phase SST stage was adopted to understand and improve the effectiveness of the proposed system. In the second section, a simulation for a specific Time interval of the day was suggested to validate the performance of the proposed management strategy.

6.1. Simulation of the three stage SST

6.1.1. Modular multilevel converter results

Table 1. Parameter Values of the SST.

Parameter name	Parameter values
Input voltage(V_g)	320 KV
Output voltage of MMC converter (V_{DC})	640 KV
Series inductor (R_{arm}, L_{arm})	(1.02Ω, 50mH)
The DAB's input voltage (V_{DAB1})	1600V
The DAB's output voltage (V_{DAB2})	400 V
Number of submodules	N= 400
L_{DAB}	0.0102mH
(R_t, L_t)	(0.1Ω, 25mH)
C_{dc0}	25e-6 F
(R, L)	(0.5Ω, 60mH)
C1	39 µF

To analyze the efficiency of the energy-based control method, a ramp of 1000MW was applied to the reference value of the active power (P_{AC_ref}=1000MW) and (Q_{ref}=0) at t=0.3s. As presented in Fig. 11, the current of the grid (igd_{ref}) is generated after the application of a power ramp at (t=0.3s).
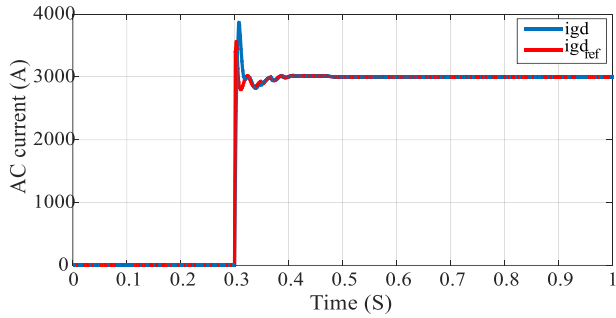
Fig. 11. MMC's grid current Behavior.
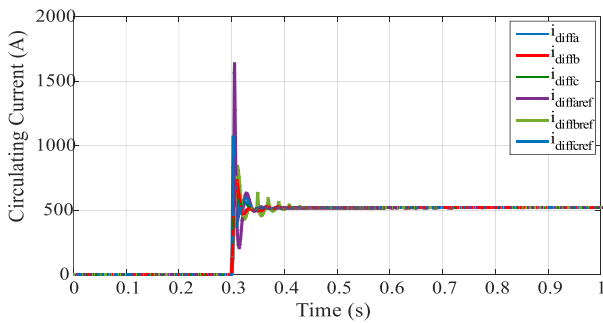
Fig. 12. MMC's circulating current behavior.

The circulating current of the phase (a, b, c) were stabilized at 510A as shown in Fig. 12. Fig. 13 depicts that the energy stored in phases (a, b, c) follows successfully its respective reference value and this can improve the performance of the differential control.
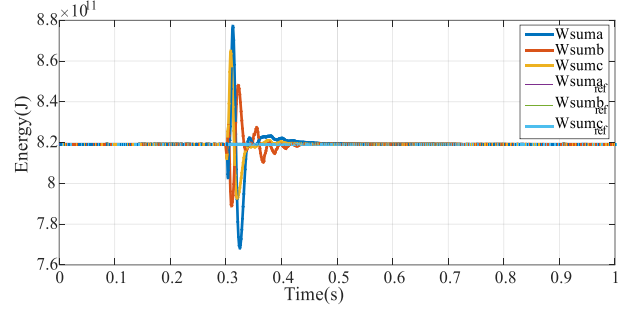
Fig.13. MMC's stored energy behavior.

The voltages (V_{cutot} et V_{cltot}) were perfectly regulated as it is shown in Fig. 14. In fact, they are stabilized at about 640KV at t=0.4s.
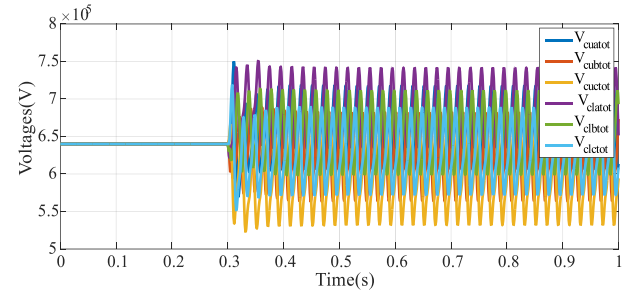
Fig. 14. Evolution for the arm voltages of MMC.

6.1.2. *Dual active bridge converter results*

The DC/DC isolation stage generates two square voltages, V_{T1} and V_{T2}, on the primary and secondary sides of the high-frequency transformer. A phase-shift (θ) is introduced between the switching signals for the primary side and the switching signals for the secondary side, leading to the same phase-shift between the two voltages V_{T1} and V_{T2}. According to Fig. 15, we can deduce that the square voltages will always have duty cycles of 50% of the switching period while the frequency stays constant which confirms the soft-switching process's operation.
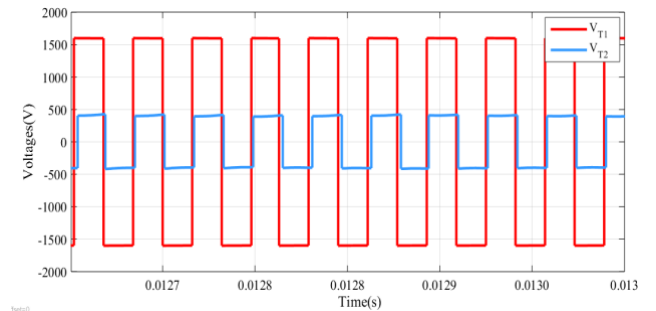
Fig. 15. Primary and secondary voltages of the HT.

The DAB converter's input and output voltages are 1600V and 400V, respectively, as depicted in Fig. 16 and Fig. 17.
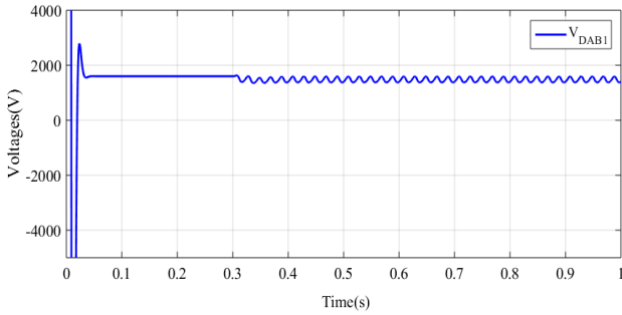
Fig.16. The DAB converter's input voltage.
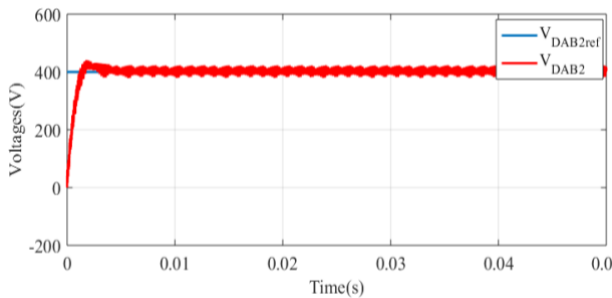
Fig.17. The DAB converter's output voltage.

6.1.3. Three phase inverter results

The Three-Phase inverter serves to connect the SST to the LV-grid and converts the DC voltage V_{DAB2} to an AC voltage by controlling the amplitude and phase shift of the generated AC voltage. Fig. 18 displays the currents i_{s1}, i_{s2}, and i_{s3} required by the three-phase AC load.
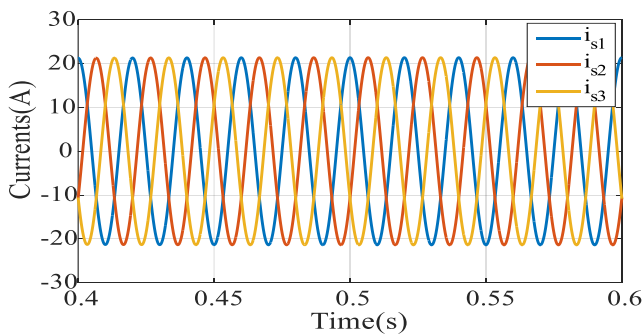
Fig. 18. Currents demanded by the three-phase AC load.

Fig. 19 shows the three modulated voltages $V_{m1}, V_{m2}, and V_{m3}$ at the inverter's output. As shown in Fig.18 and Fig. 19, the synchronization of voltage and current waveforms in the output stage of the SST ensures reactive power compensation, leading to an enhancement in voltage stability.
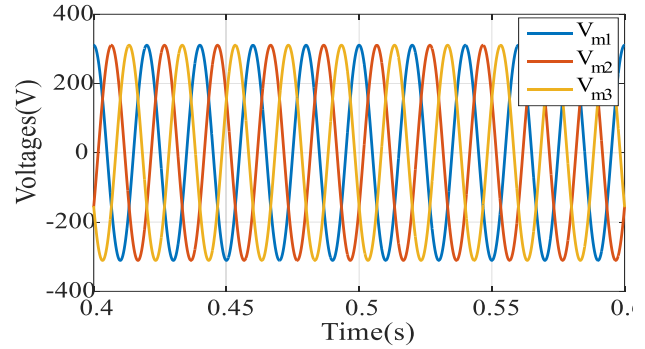
Fig.19. The three modulated voltages at the output of the inverter.

6.2. Energy Management Strategy Results

In this work, the size of the PV panel corresponding to each subsystem is related to the annual energy consumption; therefore, the studied system consists of: 4.5KWc of PV power for the subsystem1, 2.5KWc of PV power for the subsystem 2, 1.5KWc of PV power for the subsystem 3. The battery bank has a 260 Ah storage capacity, a two-day autonomy range, and a 50% depth of discharge. The DC/DC converter connects the storage system to the DC bus voltage, which is set at 400 V.

In order to justify the effectiveness of the proposed control management strategy and the convergence of the adopted algorithm, simulation results were presented under different conditions. The analysis of various scenarios was performed using the estimated power generation from each PV source, along with the load profile required for each AC load, as illustrated in Fig. 20. In order to regulate the power flow in a cluster of an LVDC micro-grid under four operational states, the proposed algorithm relies on data concerning the PV power related to each subsystem, the corresponding necessary power, and the SOC of the battery.
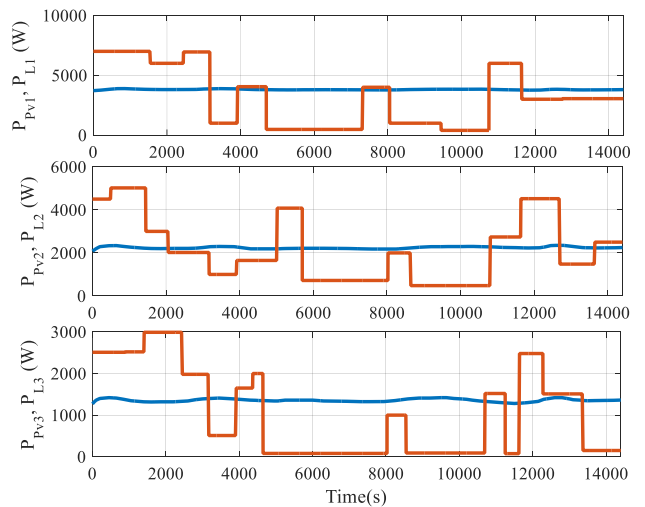
Fig. 20. Photovoltaic produced power and the demanded power load.

Fig. 21 illustrate the four interactive operational modes of the proposed management strategy. All modes are considered, and their sum equals 1. This effectively demonstrates the convergence of our algorithm, which ensures power sharing among various system elements, thereby maintaining a power balance in response to variations in PV power and demand.
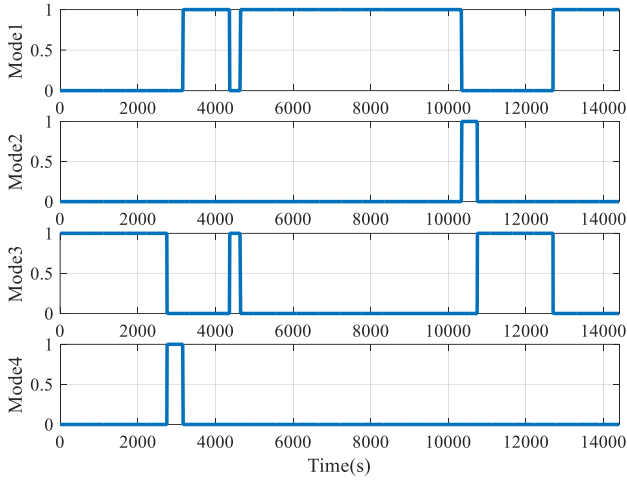
Fig. 21. Different operating modes.

Fig. 22 illustrates the state of the different operating cases; this figure shows the transfer of PV energy between the three PV subsystems that are connected together through three DC buses in the DC microgrid. The various cases presented in the algorithm enforce energy sharing among the different PV panels and illustrate the cooperative energy interaction between different subsystems to maximize the system's energy efficiency.
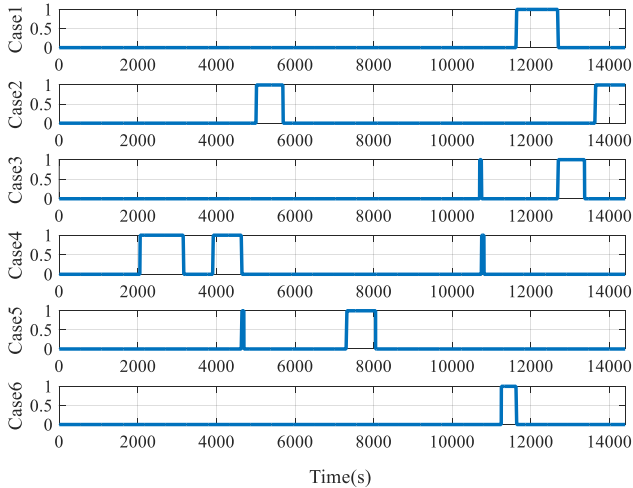
Fig. 22. State of the Different operating cases.

Fig. 23 illustrates the battery storage system's SOC. As shown in this figure, the state of charge of the battery is already maintained within its limit values ($SOC_{min} = 0.4$ and $SOC_{max} = 0.9$).
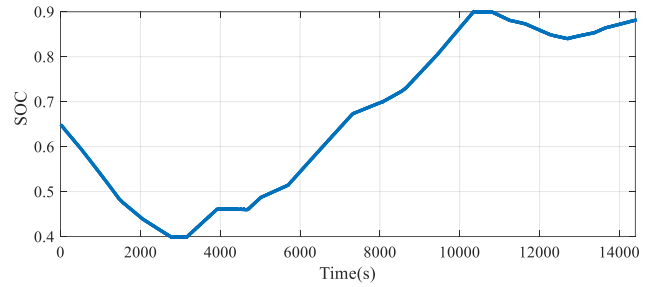
Fig.23. Battery storage system's SOC.

Fig. 24 depicts the power exanched by the LVAC grid. When the SoC reaches its minimum value, it indicates that the battery is completely discharged, resulting in a deficit that needs to be covered by the grid. Conversely, when the SoC reaches its maximum value, it signifies that the battery is fully charged, and thus, excess energy must be sent back to the grid to maintain a power balance.
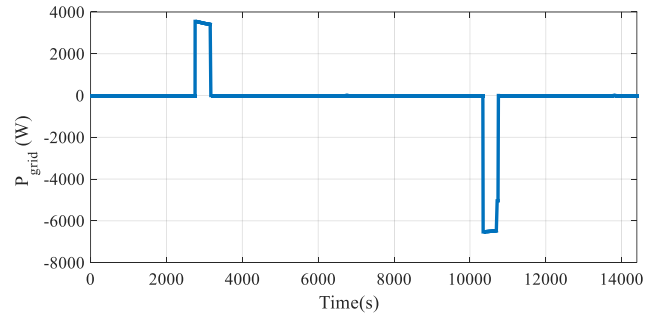
Fig.24. The power exchanged by the LVAC grid.

- In the interval [0, 2060s], there is a lack of energy in the 3 subsystems, this indicates that the produced PV energy in each subsystem is lower than the corresponding requested energy, as depicted in Fig. 20, the battery must compensate the lack of power since the state of charge does not reach its minimum value as shown in Fig. 23: Mode3 is activated.
- In the intervals [2060, 2750s] and [4370, 4650s], there is a lack of energy in subsystems 1 and 3 while subsystem 2 has an excess. The surplus energy is redistributed from subsystem 2 to other subsystems that require it: Mode 3 and case 4 are activated. Since this excess energy cannot completely satisfy the needs of subsystems 1 and 3, the battery must be discharged to cover the lack of energy as shown in Fig. 25. When the state of charge of the battery reaches its minimum value $SOC = SOC_{min} = 0.4$, the lack of energy must be covered by the LVAC grid as shown in Fig. 24: Mode 4 is activated in the interval [2750s-3170s].
- In the intervals [3170, 4370s], [4650, 5020s], [5700, 7320s], [8050, 10350s], there is an excess of energy in the 3 subsystems, which indicates that the produced PV energy in each subsystem is greater than the corresponding requested, the excess energy is directed back to charge the battery as long as its state of charge remains below its maximum value, as shown in Fig. 23: mode1 is activated.
- In the intervals [5020, 5700s], there is a lack of energy in subsystem 2 while subsystems 1 and 3 have an excess. This energy excess is transferred to subsystem 2 in order

to meet his needs through the DC microgrid. In this situation, once the energy demand is fulfilled, and there is still an excess of energy available, this surplus is directed towards charging the battery: Mode 1 and case 2 are activated. The same conditions apply for the interval [7320, 8050s] when there is a lack of energy in subsystem 1 while subsystems 2 and 3 have an excess: mode 1 and case 5 are activated. When the state of charge of the battery reaches its maximum value $SOC = SOC_{max} = 0.9$, the excess of energy must be transferred to the LVAC grid as it is shown in Fig. 24: Mode 2 is activated in the interval [10350, 10750s].
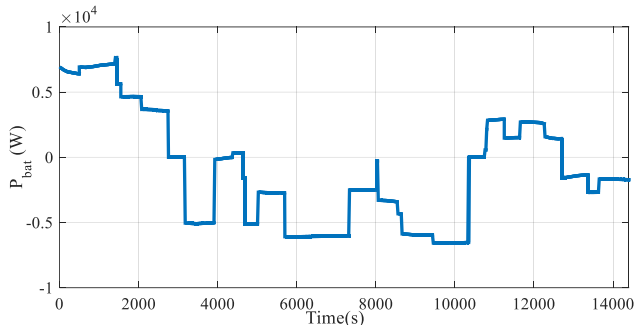
Fig. 25. Battery storage system's power.

In the presented system, different components are well-connected through the DC bus, and the proposed algorithm demonstrates power balance under various conditions. Fig. 26 illustrates the DC bus voltage profile, which remains constant and follows its reference value. Therefore, the system simulation proves the efficacity of the proposed control strategy in maintaining power balance across the various system components, even when confronted with different scenarios of generated PV power and load demand.
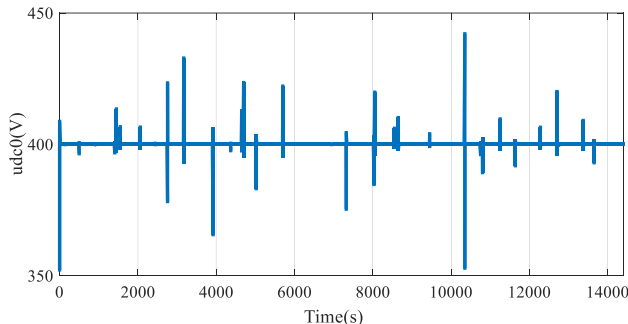
Fig.26. DC bus voltage.

7. Conclusion

This paper focuses on the development of an efficient control strategy for an LVDC distribution system, employing a three-stage SST as its key element. The SST, with its MMC at the input, DAB converter in the middle, and three-phase inverter at the output, forms a resilient and efficient interface between various voltage levels and grid systems. This architecture aligns seamlessly with smart grid integration, offering reliability and effectiveness.
Furthermore, the LVDC microgrid (µG) interconnected with the SST enhances the overall system's efficiency and

power quality. It accomplishes this by regulating and stabilizing voltage levels, facilitating the integration of renewable energy sources, and promoting energy sustainability. The study introduces a global supervisory control strategy for the LVDC µG, facilating coordination among various smart grid components. Our algorithm effectively manages power flow across the various elements of the hybrid system, ensuring power balance and energy cooperation among the three subsystems to optimize the use of PV power.

This research aims to enhance system performance, minimize reliance on storage systems, , alleviate the pressure on the main grid, and highlight the crucial role of LVDC based on SST architecture in advancing the future of energy distribution and sustainability.

References

[1] M. Abdou-Tankari, G. Lefebvre, J. Arkhangelski, A. Drame, M. Garba, and D. Abdourahimou, "Power quality challenges and urban microgrid based grid resiliency.", IEEE International Conference on Renewable Energy Research and Applications (ICRERA)

[2] S. Goud, T. V. S. Kalyani, K. V. G. Rao, and G. J. I. J. o. S. G.-i. Sanjeev, "Amalgamation of Smart Grid with Renewable Energy Sources", International Journal of Smart Grid (ijSmartGrid), vol. 7, no. 2, pp. 103-107, 2023.

[3] M. Cakir, I. Cankaya, I. Garip, and I. Colak, "Advantages of Using Renewable Energy Sources in Smart Grids." 10th International Conference on Smart Grid (icSmartGrid), pp. 436-439.

[4] A. M. Colak, and O. Kaplan, "A review on the efficiency increment in a power system using smart grid technologies", 2021 9th International Conference on Smart Grid (icSmartGrid), pp. 192-196.

[5] R. Kallel, and G. J. J. o. B. E. Boukettaya, "An energy cooperative system concept of DC grid distribution and PV system for supplying multiple regional AC smart grid connected houses", 2022 Journal of Building Engineering (JBE), vol. 56, pp. 104737.

[6] A. Perera, V. M. Nik, P. Wickramasinghe, and J.-L. J. A. E. Scartezzini, "Redefining energy system flexibility for distributed energy system design," Applied Energy, vol. 253, pp. 113572, 2019.

[7] M. J. O. Panão, N. M. Mateus, and G. C. J. A. E. Da Graça, "Measured and modeled performance of internal mass as a thermal energy battery for energy flexible residential buildings", Applied Energy, vol. 239, pp. 252-267, 2019.

[8] S. S. Shah, and S. J. I. T. o. I. E. Bhattacharya, "A simple unified model for generic operation of dual active bridge converter", IEEE Transactions on Industrial Electronics, vol. 66, no. 5, pp. 3486-3495, 2018.

[9] V. Vita, C. Christodoulou, I. Zafeiropoulos, I. Gonos, M. Asprou, and E. J. A. S. Kyriakides, "Evaluating the flexibility benefits of smart grid innovations in transmission networks", Applied Sciences, vol. 11, no. 22, pp. 10692, 2021.

[10]   P.-H. Li, and S. J. A. e. Pye, "Assessing the benefits of demand-side flexibility in residential and transport sectors from an integrated energy systems perspective", Applied energy vol. 228, pp. 965-979, 2018.

[11]   M. Meliani, A. E. Barkany, I. E. Abbassi, A. M. Darcherif, and M. J. I. J. o. E. B. M. Mahmoudi, "Energy management in the smart grid: State-of-the-art and future trends", International Journal of Engineering Business Management, vol. 13, pp. 18479790211032920, 2021.

[12]   H. Shadfar, M. Ghorbani Pashakolaei, and A. J. I. T. o. E. E. S. Akbari Foroud, "Solid-state transformers: An overview of the concept, topology, and its applications in the smart grid", International Transactions on Electrical Energy Systems, vol. 31, no. 9, pp. e12996, 2021.

[13]   S. Saleh, C. Richard, X. S. Onge, K. McDonald, E. Ozkop, L. Chang, and B. Alsayid, "Solid-state transformers for distribution systems: Technology, performance, and challenges", 55th Industrial and Commercial Power Systems, pp. 1-15, 2019

[14]   M. A. Hannan, P. J. Ker, M. S. H. Lipu, Z. H. Choi, M. S. A. Rahman, K. M. Muttaqi, and F. J. I. A. Blaabjerg, "State of the art of solid-state transformers: Advanced topologies, implementation issues, recent progress and improvements", Ieee Access, vol. 8, pp. 19113-19132, 2020.

[15]   M. S. Mollik, M. A. Hannan, M. S. Reza, M. S. Abd Rahman, M. S. H. Lipu, P. J. Ker, M. Mansor, and K. M. J. E. Muttaqi, "The Advancement of Solid-State Transformer Technology and Its Operation and Control with Power Grids: A Review", Electronics ,vol. 11, no. 17, pp. 2648, 2022.

[16]   A. Rehman, M. Imran-Daud, S. K. Haider, A. U. Rehman, M. Shafiq, and E. T. J. S. Eldin, "Comprehensive Review of Solid State Transformers in the Distribution System: From High Voltage Power Components to the Field Application", Symmetry, vol. 14, no. 10, pp. 2027, 2022.

[17]   S. Khan, K. Rahman, M. Tariq, S. Hameed, B. Alamri, and T. S. J. S. Babu, "Solid-State Transformers: Fundamentals, Topologies, Applications, and Future Challenges", Symmetry vol. 14, no. 1, pp. 319, 2021.

[18]   M. F. Fiaz, S. Calligaro, M. Iurich, and R. J. E. Petrella, "Analytical Modeling and Control of Dual Active Bridge Converter Considering All Phase-Shifts", Energies vol. 15, no. 8, pp. 2720, 2022.

[19]   D. K. Mishra, M. J. Ghadi, L. Li, M. J. Hossain, J. Zhang, P. K. Ray, A. J. I. J. o. E. P. Mohanty, and E. Systems, "A review on solid-state transformer: A breakthrough technology for future smart distribution grids", International Journal of Electrical Power & Energy Systems vol. 133, pp. 107255, 2021.

[20]   Y. Li, Y. Zhang, R. Cao, X. Liu, C. Lv, J. J. C. T. o. P. E. Liu, and Applications, "Redundancy design of modular DC solid-state transformer based on reliability and efficiency evaluation", CPSS Transactions on Power Electronics and Applications, vol. 6, no. 2, pp. 115-126, 2021.

[21]   D. Cervero, M. Fotopoulou, J. Muñoz-Cruzado, D. Rakopoulos, F. Stergiopoulos, N. Nikolopoulos, S. Voutetakis, and J. F. J. E. Sanz, "Solid State Transformers: A Critical Review of Projects with Relevant Prototypes and Demonstrators", Electronics, vol. 12, no. 4, pp. 931, 2023.

[22]   N. Hugo, P. Stefanutti, M. Pellerin, and A. Akdag, "Power electronics traction transformer", European conference on power electronics and application, pp. 1-10, 2007

[23]   F. Ruiz, M. A. Perez, J. R. Espinosa, T. Gajowik, S. Stynski, and M. J. I. I. E. M. Malinowski, "Surveying solid-state transformer structures and controls: Providing highly efficient and controllable power flow in distribution grids", IEEE Industrial Electronics Magazine, vol. 14, no. 1, pp. 56-70, 2020.

[24]   I. E. Davidson, and E. Buraimoh, "Modeling and Fault Ride-Through Control Strategy for Grid-Supporting Photovoltaic-Based Microgrids", International Journal of Smart Grid (isSmartGrid), vol. 7, June, 2023

[25]   T. Isobe, R. A. Barrera-Cardenas, Z. He, Y. Zou, K. Terazono, H. J. I. J. o. E. Tadano, and S. T. i. P. Electronics, "Control of three-phase solid-state transformer with phase-separated configuration for minimized energy storage capacitors", IEEE Journal of Emerging and Selected Topics in Power Electronics ,vol. 8, no. 3, pp. 3014-3028, 2019.

[26]   Z. Li, T. Zheng, Y. Wang, and C. J. A. S. Yang, "A Hierarchical Coordinative Control Strategy for Solid State Transformer Based DC Microgrids", Applied Sciences, vol. 10, no. 19, pp. 6853, 2020.

[27]   L. Zheng, A. Marellapudi, V. R. Chowdhury, N. Bilakanti, R. P. Kandula, M. Saeedifard, S. Grijalva, D. J. I. J. o. E. Divan, and S. T. i. P. Electronics, "Solid-state transformer and hybrid transformer with integrated energy storage in active distribution grids: Technical and economic comparison, dispatch, and control", IEEE Journal of Emerging and Selected Topics in Power Electronics, vol. 10, no. 4, pp. 3771-3787, 2022.

[28]   L. Zheng, R. P. Kandula, and D. J. I. T. o. P. E. Divan, "Current-source solid-state DC transformer integrating LVDC microgrid, energy storage, and renewable energy into MVDC grid", IEEE Transactions on Power Electronics, vol. 37, no. 1, pp. 1044-1058, 2021.

[29]   X. Zhao, B. Li, Q. Fu, S. Mao, D. Xu, J. I. Leon, and L. G. J. I. T. o. P. E. Franquelo, "DC solid state transformer based on three-level power module for interconnecting MV and LV DC distribution systems", IEEE Transactions on Power Electronics vol. 36, no. 2, pp. 1563-1577, 2020.

[30]   F. Vaca-Urbano, M. S. Alvarez-Alvarado, A. A. Recalde, and F. Moncayo-Rea, "Solid-state transformer for energy efficiency enhancement", Research Trends and Challenges in Smart Grids: IntechOpen, 2019.

[31]   I. Patrao, E. Figueres, G. Garcerá, R. J. R. González-Medina, and S. E. Reviews, "Microgrid architectures for low voltage distributed generation", Renewable and Sustainable Energy Reviews, vol. 43, pp. 415-424, 2015.

[32] W. Rodrigues, R. Santana, A. Cota, T. Oliveira, L. Morais, and P. Cortizo, "Integration of solid state transformer with DC microgrid system", IEEE 2nd Annual Southern Power Electronics Conference (SPEC), pp. 1-6, 2016.

[33] M. Liserre, G. Buticchi, M. Andresen, G. De Carne, L. F. Costa, and Z.-X. J. I. I. E. M. Zou, "The smart transformer: Impact on the electric grid and technology challenges", IEEE Industrial Electronics Magazine vol. 10, no. 2, pp. 46-58, 2016.

[34] A. Ismail, M. S. Abdel-Majeed, M. Y. Metwly, A. S. Abdel-Khalik, M. S. Hamad, S. Ahmed, E. Hamdan, and N. A. J. A. S. Elmalhy, "Solid-state transformer-based DC power distribution network for shipboard applications", Applied Sciences vol. 12, no. 4, pp. 2001, 2022.

[35] L. F. Costa, G. De Carne, G. Buticchi, and M. J. I. P. E. M. Liserre, "The smart transformer: A solid-state transformer tailored to provide ancillary services to the distribution grid", IEEE Power Electronics Magazine vol. 4, no. 2, pp. 56-67, 2017.

[36] S. Samimi, "Modélisation et Commande des Convertisseurs MMC en vue de leur Intégration dans le Réseau Electrique", Doctoral dissertation, Ecole centrale de Lille, 2016.

[37] S. Du, A. Dekka, B. Wu, and N. Zargari, *Modular multilevel converters: analysis, control, and applications*: John Wiley & Sons, Book, 2018.

[38] E. Rodriguez-Diaz, M. Savaghebi, J. C. Vasquez, and J. M. Guerrero, "An overview of low voltage DC distribution systems for residential applications.", IEEE 5th International Conference on Consumer Electronics-Berlin (ICCE-Berlin). IEEE, pp. 318-322, 2015.

[39] H. Ataullah, T. Iqbal, I. U. Khalil, U. Ali, V. Blazek, L. Prokop, and N. J. E. Ullah, "Analysis of the Dual Active Bridge-Based DC-DC Converter Topologies, High-Frequency Transformer, and Control Techniques", Energies, vol. 15, no. 23, pp. 8944, 2022.

[40] S. Saeed, and J. Garcia, "Extended operational range of dual-active-bridge converters by using variable magnetic devices", IEEE Applied Power Electronics Conference and Exposition-APEC, pp. 1629-1634, 2019.

[41] V. Steub, "Study of modulation schemes for the dual-active-bridge converter in a grid-conneced photovoltaic park", Master thesis, 2018.

[42] W. A. Rodrigues, T. R. Oliveira, L. M. Morais, and A. H. J. E. Rosa, "Voltage and power balance strategy without communication for a modular solid state transformer based on adaptive droop control", vol. 11, no. 7, pp. 1802, 2018.

[43] K. George, "Design and control of a bidirectional dual active bridge DC-DC converter to interface solar, battery storage, and grid-tied inverters,", Departement of electrical engineering, Thesis, 2015.

[44] F. L. Marcelino, H. H. Sathler, T. R. de Oliveira, and P. F. Donoso-Garcia, "Modeling and control of a Dual Active Bridge for energy storage in DC microgrid applications", IEEE 8th International Symposium on Power Electronics for Distributed Generation Systems (PEDG), pp. 1-8, 2017.

[45] A. Shri, "A solid-state transformer for interconnection between the medium-and the low-voltage grid", Departement of electrical engineering, Master Thesis, Delft University of Technology, 2013.

[46] H. Qin, and J. W. J. I. T. o. p. e. Kimball, "Generalized average modeling of dual active bridge DC–DC converter", IEEE Transactions on power electronics, vol. 27, no. 4, pp. 2078-2084, 2011.

[47] P. Münch, D. Görges, M. Izák, and S. Liu, "Integrated current control, energy control and energy balancing of modular multilevel converters", Annual Conference on IEEE Industrial Electronics, pp. 150-155, 2010.

[48] R. Asma, G. François, and B. Ghada, "Modelling, Control and simulation of an MMC applied to a point to point HVDC system", 6th IEEE International Energy Conference (ENERGYCon) pp. 164-169, 2020.